bioresources.com

Experimental Static and Seismic Behaviour of Glulam Beam-to-Column Connection with Screwed-in Threaded Rod Joints

Huifeng Yang,[a,*] Chaochao Wang,[a] Junbin Hu,[a] Haotian Tao,[b] Jiwei Liu,[b] Liqiu Tang,[a] and Benkai Shi [a]

To evaluate the static and seismic behaviour of glulam beam-to-column connections with screwed-in threaded rods, nine specimens grouped in three were tested under both monotonic and reversed cyclic loads. The failure modes, moment resistance, initial rotation stiffness, ductility, and energy dissipation capacity of the developed connections were investigated. The results indicated that the developed beam-to-column connections showed superior structural performance. Furthermore, with the introduction of a steel bracket, the hybrid screwed-in threaded rod connection features larger stiffness, higher load-carrying capacity, remarkable ductility, and better energy dissipation capacity. The main failure modes included the yielding of steel brackets, as well as the yielding or rupture of the threaded rods, which indicated a ductile behaviour. The connection specimens with steel columns showed larger stiffness than those with glulam columns, which is reasonable for the bigger compressive deformation of glulam columns.

*Contact information: a: College of Civil Engineering, Nanjing Tech University, Nanjing, 211816, China; b: School of Civil Engineering, Southeast University, Nanjing, 211189, China; * Corresponding authors: hfyang@njtech.edu.cn; yhfbloon@163.com*

INTRODUCTION

Joints and connections play extremely important roles in structural timber and steel design. For timber structures, the resistance, ductility, and energy dissipation depend on the connections (Xu *et al*. 2009; Leijten 2011; Liu and Yang 2019). With the increasing application of timber structures in multi-story and long-span structures, it is necessary to develop new types of jointing or connection systems to meet the needs of prefabrication, efficiency, high performance, *etc*.

The dowel-type connection is widely used in timber structures for its good economic performance, convenient assembly, and reliable force transmission (Liu and Yang 2019). However, traditional dowel-type connections show significant limitations on the connection load-carrying capacity and stiffness (Lam *et al*. 2010; Araki *et al*. 2011; Wang *et al*. 2015). As a result, it is usually considered as a hinge connection (Li *et al*. 2021), which deeply restricts the development of multi-story and long-span structures.

To obtain a ductile moment-resisting connection and meet the needs of high performance connection for timber structures, a large amount of research effort has been made. Typically, glued-in rod connections are introduced to timber structures. The primary attractive properties of this sort of connection include high load-carrying capacity, high stiffness, and aesthetic appearance (Yang *et al*. 2016). Buchanan and Fairweather (1993)

investigated moment-resisting glulam beam-column connections with glued-in rods. Their results showed that the connection has a high level of moment resistance. Furthermore, while combined with some steel brackets, it can further overcome the environmental restrictions for glued-in rod connections, as the gluing process is conducted in an indoor environment. As another benefit from the introduction of the steel brackets, it allows a practical application and easy assembly (Yang *et al*. 2016).

A great deal of research work has been carried out on moment-resisting hybrid connections including finite element analysis (Vašek and Vyhnálek 2006), theoretical evaluation (Vašek and Vyhnálek 2006; Yang *et al*. 2016), and design process (Fragiacomo and Batchelar 2012a,b). Nevertheless, the gluing quality control is a potential problem, and the evaluation of durability behaviour of glued-in rod connections is still inadequate. Therefore, the application of glued-in rod connections in timber structures is restricted.

The screwed-in threaded rod joint is an axially loaded mechanically fastened joint, featuring large stiffness and high load-carrying capacity. With the development of screwed-in threaded rod joints and connections, the above existing problems for glued-in rod connections can be solved very well. Considerable research on the withdrawal behaviour of screwed-in threaded rod joints has been conducted. There have been experimental, numerical, and theoretical investigations of withdrawal capacity and stiffness of threaded rods screwed-in glulam timber (Stamatopoulos and Malo 2015; Stamatopoulos and Malo 2016; Stamatopoulos and Malo 2018; Stamatopoulos and Malo 2020; Yang *et al*. 2021). A model based on non-linear fracture mechanics has been used to estimate the withdrawal capacity of screws embedded in glulam (Jensen *et al*. 2012).

Some research has been undertaken on moment-resisting joints using screwed-in threaded rod. A moment-resisting joint system using screwed-in threaded rods (lagscrewbolt) shows high performance (Nakatani *et al*. 2006). Experimental, analytical, and numerical method were used to gauge the performance of a semirigid timber frame with screwed-in threaded rods (Mori *et al*. 2015). Both the analytical and numerical model showed good agreement with the experimental results. Based on previous studies, a hybrid moment-resisting joint system that combined screwed-in threaded rods and slotted bolted connection was presented (Komatsu *et al*. 2018). The developed hybrid joint features high initial stiffness, good yielding capacity, and considerable ductility.

In this work, a hybrid connection consisting of screwed-in threaded rod and steel brackets was developed. A series of monotonic and reversed cycle loading tests were implemented to evaluate the static and seismic performance. In addition, the failure modes, load-carrying capacity, initial stiffness, ductility, and energy dissipation capacity of the connections were evaluated.

EXPERIMENTAL

Materials

The physical and mechanical properties of the glulam elements are shown in Table 1. The characteristic yield strength of the threaded rods is 800 MPa. The outer and root thread diameter of the rods are 20 mm and 15 mm, respectively. The steel bracket, which is designed to connect beam to column elements in some specimens, was fabricated using grade of Q235 with the yield strength of 235 MPa (GB/T 50017 2017). The strength grade of anchoring bolts are 8.8 with the yield strength of 640 MPa.

bioresources.com

Table 1. Physical and Mechanical Properties of Glulam

Material	Density (g/cm^3)	Moisture content (%)	Tensile strength parallel to grain (MPa)	Compressive strength parallel to grain (MPa)	Young's modulus (MPa)
Douglas fir	0.531	15.2	52.2	46.3	13020

Sample Preparation

As shown in Figs. 1(a), 1(b), and 1(c), the test series were divided into three groups (T1, T2, and T3) of three T-shaped beam-to-column connection specimens each. The column elements in groups T1 and T2 employed H-section steel, while the one in group T3 was glulam. Both the glulam beam and column elements were made from Douglas fir lumber pieces. The dimensions of the glulam beam and column elements were 1500 mm (length) × 135 mm (width) × 420 mm (depth) and 1500 mm (height) × 150 mm (width) × 350 mm (depth), respectively. The outline dimensions of the steel column were 1500 mm (height) × 160 mm (flange's width) × 350 mm (cross sectional depth). The steel brackets in groups T2 and T3 were designed as energy dissipating elements, which resulted in fast assembly of the structures.

The embedment length of the threaded rods at the upper and lower position of the beam section was 400 mm for mainly resisting the moment by utilizing the high withdrawal properties of the rods, while that of the rod at the middle position of the section was 200 mm to mainly transfer the shearing force (see Fig. 1). The threaded rods were drilled into the glulam beams through predrilled holes with diameters of 15 mm by using a torque wrench, and the detailed geometry dimensions of the threaded rods are shown in Fig. 2. It should be noted that according to the preliminary pull-out test results conducted by the authors, the four threaded rods at one side provided high ultimate withdrawal capacity larger than 350 kN and elastic stiffness greater than 70 kN/mm, respectively. To match the torque wrench and nut, the screwed-in part at the extended end of the rods was processed into a square head, followed by a bolted thread part, as shown in Fig. 2 (Yang *et al*. 2021). To reduce or prevent the splitting failure of the glulam beam end, three rows of 6 self-tapping screws (VGZ7180) at the top surface and two rows of 4 self-tapping screws (VGZ7100) at side surface were screwed into the glulam beams perpendicular to the grain, as illustrated in Fig. 1(d).

Both static monotonic and reversed cycle loading tests were conducted for each group, in which one specimen was tested under static monotonic loading test and the other two were tested under reversed cycle loading test. Therefore, the subgroup was defined, which include MT1, MT2, MT3, CT1, CT2, and CT3. Take group T1 as an example, the specimens tested under static monotonic load was named as MT1, while the other two under reversed cycle load as CT1-1 and CT1-2, respectively.
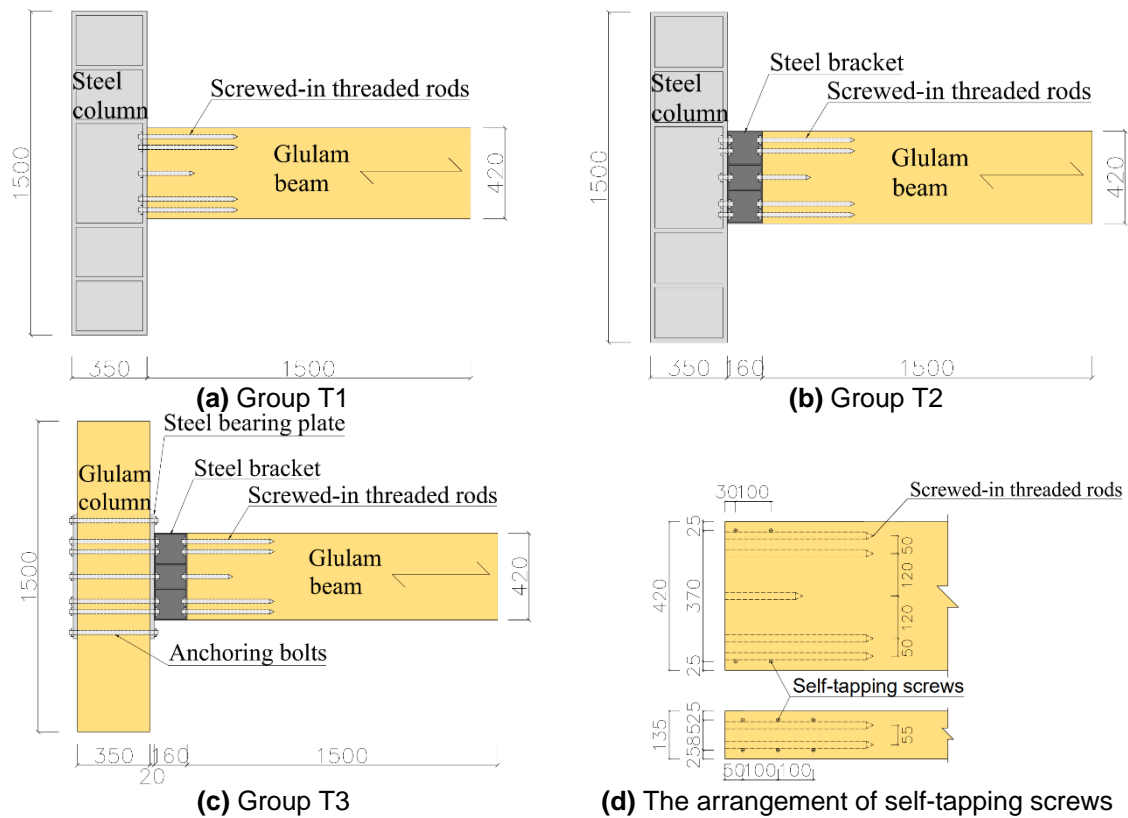
(a) Group T1

(b) Group T2

(c) Group T3

(d) The arrangement of self-tapping screws
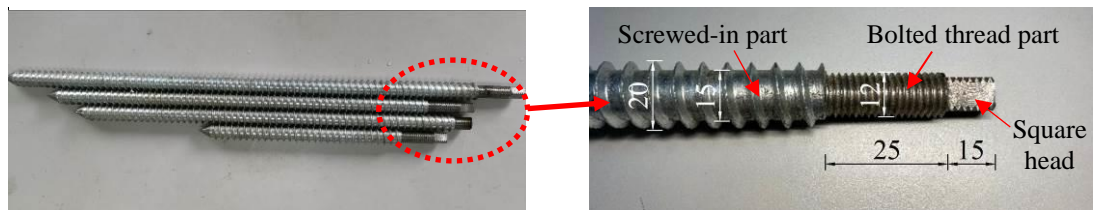
Fig. 1. Schematic of specimens

Fig. 2. Geometry of the threaded rods (Yang *et al*. 2021)

Methods

The test setup is schematically illustrated in Fig. 3. The hydraulic actuator of 250 kN capacity was connected to the cantilever end of glulam beam to apply the load. Three linear variable displacement transformers (LVDTs) were arranged to record the displacement value. As shown in Fig. 3, LVDT1 was arranged at the loading point, while LVDT2 and LVDT3 were arranged at 300 mm from the surface of the column.
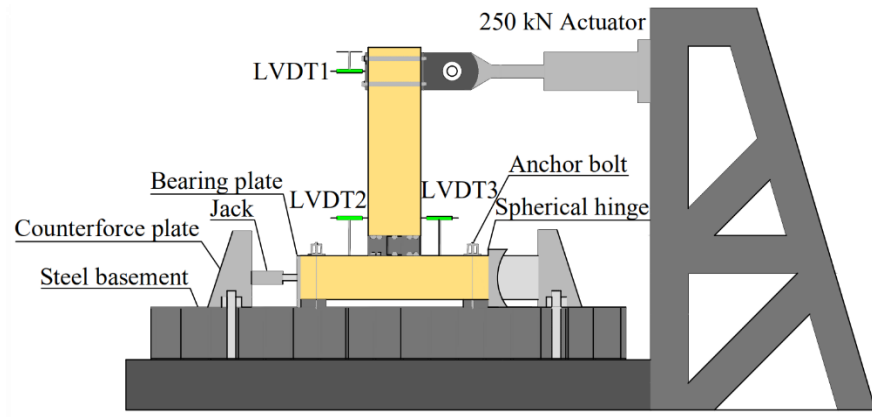
Fig. 3. Test set-up

The tests were conducted under displacement control. The specimens were loaded at a constant rate of 0.1 mm/s for monotonic loading test, while 0.3 mm/s to 2.4 mm/s for reversed cycle loading test, as presented in Table 2.

Table 2. Loading History

Load step	1	2	3	4	5	6	7	8	9	10	11	12	13	14
Peak drift angle (rad)	0.00375	0.005	0.0075	0.01	0.015	0.02	0.03	0.04	0.05	0.06	0.07	0.08	0.09	0.10
Peak deformation (mm)	5.65	7.5	11.75	15	22.5	30	45	60	75	90	105	120	135	150
Number of cycles	6	6	6	4	2	2	2	2	2	2	2	2	2	2
Loading rate (mm/s)	0.3	0.3	0.6	0.6	0.6	0.6	1.2	1.2	1.2	2.4	2.4	2.4	2.4	2.4
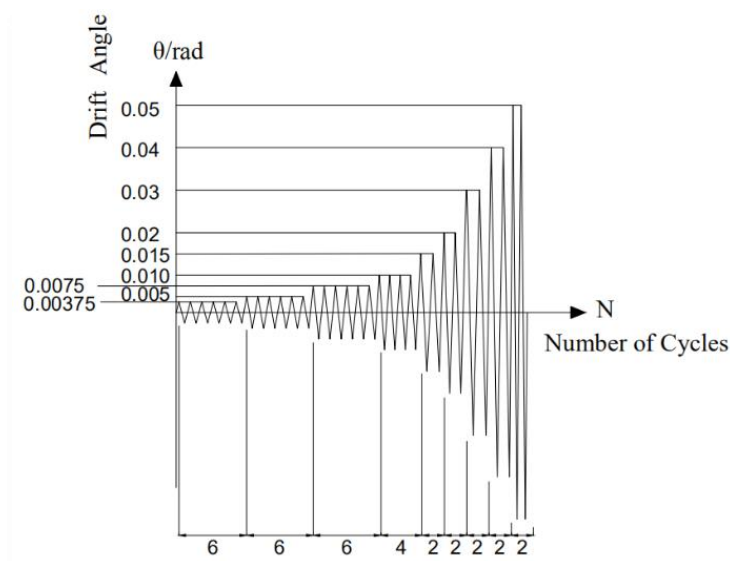
Fig. 4. Loading procedure

The cyclic loading procedure is illustrated in Fig. 4, with the loading history as shown in Table 2 (Clark *et al*. 1997). The drift angle θ can be derived from the displacement values of the beams. According to Clark *et al*. (1997), the peak drift angle θ of the first six loading steps for the reversed cycle loading test is 0.00375, 0.005, 0.0075, 0.01, 0.015, 0.02, and 0.03, respectively. Thereafter, it will continue with the increment of 0.01, and perform two cycles at each step.
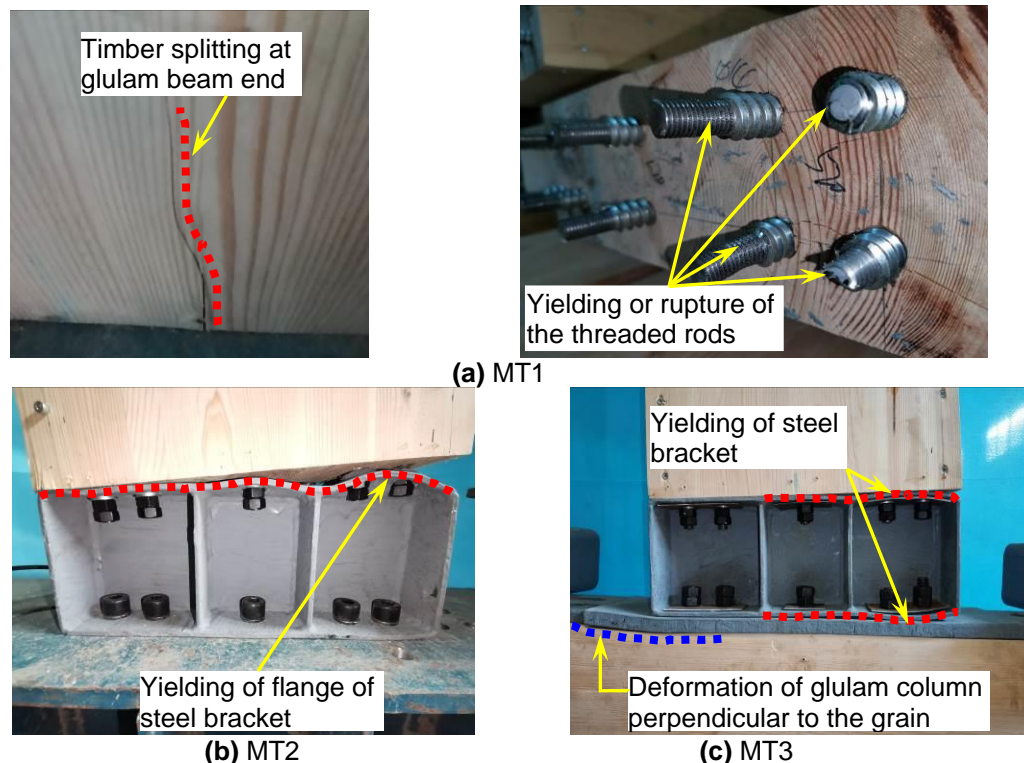
The connection drift angle could be calculated based on the geometric data of the horizontal displacement measured by the displacement gauges and the distance between the displacement gauges.

RESULTS AND DISCUSSION

Monotonic Loading Test
Failure modes

Figure 5 presents the failure modes of monotonic loading test specimens. For specimen MT1, slight splitting occurred at the beam end in the latter stage. Thereafter, the specimen could still bear the applied load until the yielding or breaking of the threaded rods, as illustrated in Fig. 5(a). The self-tapping screw reinforcement improved the anti-splitting resistance. Due to the introduction of steel brackets for the connections, the failure of specimens MT2 and MT3 was caught by the big deformation and yielding of the steel brackets (Fig. 5(b) and Fig. 5(c)). Moreover, for specimen MT3, in which the column element using glulam materials, obvious deformation occurred perpendicular to the grain of the column. Both specimens MT2 and MT3 with steel brackets showed better ductile behaviour.

Timber splitting at glulam beam end

Yielding or rupture of the threaded rods

(a) MT1

Yielding of steel bracket

Yielding of flange of steel bracket

Deformation of glulam column perpendicular to the grain

(b) MT2   **(c)** MT3

Fig. 5. Failure modes of the specimens under monotonic loading

Moment resistance

The typical moment-rotation curves at the beam end are illustrated in Fig. 6, while the main test results of the monotonic tests are listed in Table 3. As indicated in Table 3, k_s is the initial rotation stiffness of the connection M_y and M_{max} are the yielding moment and ultimate moment, respectively. θ_y and θ_{max} are the drift angles corresponding to M_y and M_{max}, respectively. and μ is the ductility factor of the connection, which is calculated by Eq. 1. It should be noted that the definition of typical parameters of the moment-rotation curve shown in Fig. 7 was obtained in accordance with EN 12512 (2001). As shown in Fig. 8, the yield values were determined by the intersection of the following two lines: the first line will be determined as that drawn through the point on the moment-rotation curve corresponding to 0.1 M_{max} and the point on the moment-rotation curve corresponding to 0.4 M_{max}; the second line is the tangent having an inclination of 1/6 of the first line (EN 12512 2001). The initial rotation stiffness is the slope of the envelope curve corresponding to between 0.1 M_{max} and 0.4 M_{max} (EN 12512 2001), as follows,

$$\mu = \theta_y / \theta_{max} \tag{1}$$

where θ_y and θ_{max} are the rotation corresponding to the yielding moment and maximum moment, respectively.

As illustrated in Fig. 6 and Table 3, both the load-carrying capacity and the initial rotational stiffness of specimen MT1 (without steel bracket) were much higher than those of specimens MT2 and MT3 (with steel brackets). Meanwhile, the ductility behaviour showed an opposite trend.
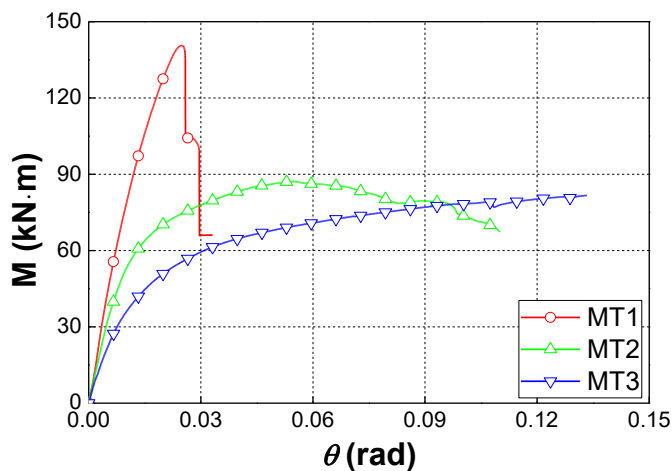

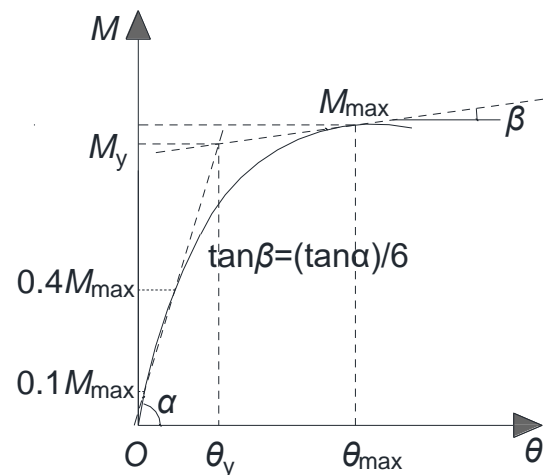**Fig. 6.** Moment (*M*)–rotation (*θ*) curves

Fig. 7. Definition of yield and maximum values

Table 3. The Main Results of the Reversed Cycle Loading Test

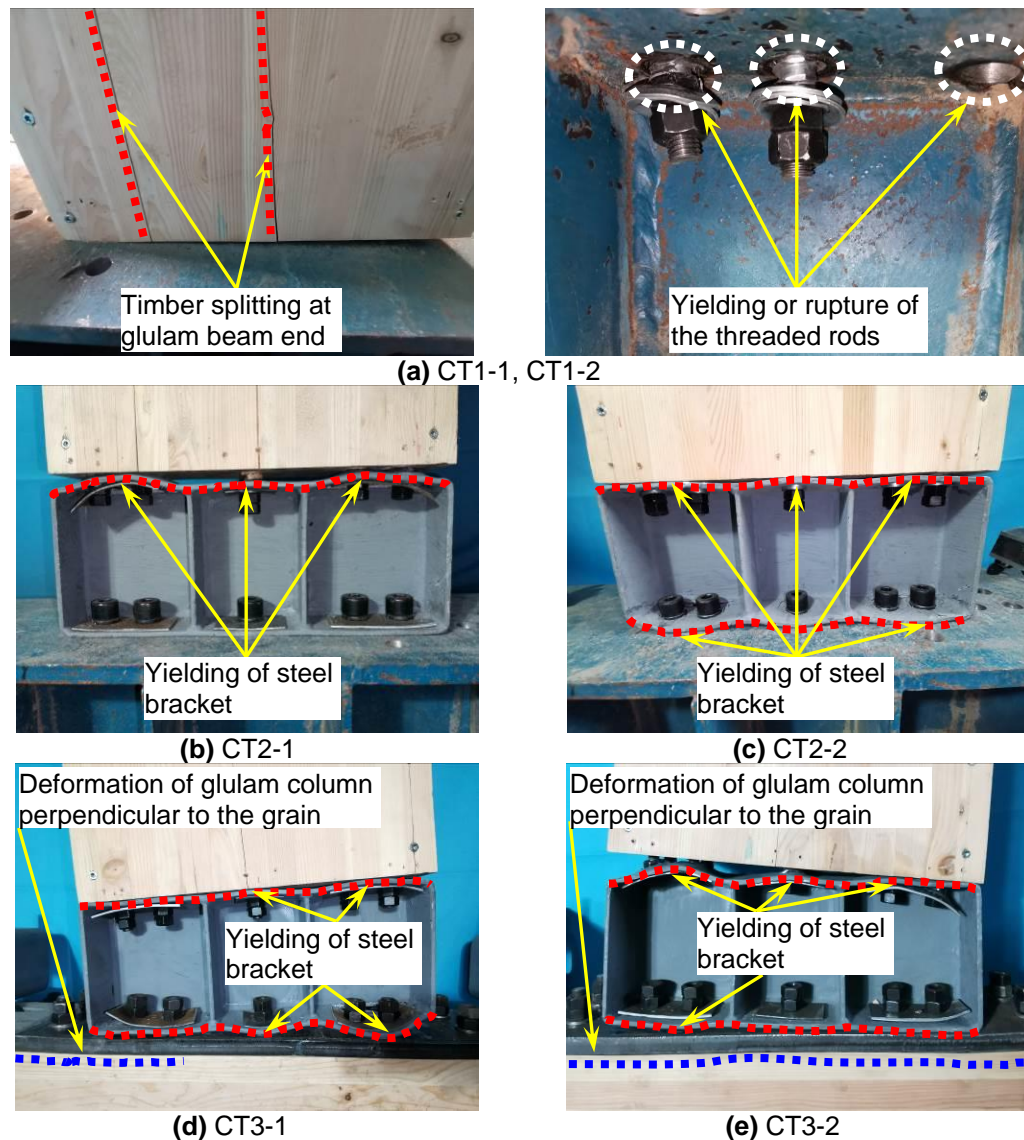| Test specimen	k_s (kN·m/rad)	θ_y (rad)	M_y (kN·m)	θ_{max} (rad)	M_{max} (kN·m)	μ
MT1	7673	0.017	127.2	0.029	140.6	1.72
MT2	6052	0.010	60.0	0.108	87.2	10.8
MT3	3473	0.013	48.4	0.133	81.7	10.2

These findings are reasonable because that the steel bracket was designed as an energy dissipating fuse element. Through an optimization of the steel bracket, the above basic structural parameters will have more compatibility. Additionally, due to the relatively low compressive stiffness perpendicular to the grain of glulam column, the initial stiffness of specimen MT3 were 42.6% lower than that of specimen MT2.

Reversed Cycle Loading Test

Failure modes

The failure modes of the specimens under reversed cycle loading tests are shown in Fig. 8. Comparing Fig. 8 with Fig. 5, the loading type has limited effects on the failure modes of the specimens.

Timber splitting at glulam beam end

Yielding or rupture of the threaded rods

(a) CT1-1, CT1-2

Yielding of steel bracket

(b) CT2-1

Yielding of steel bracket

(c) CT2-2

Deformation of glulam column perpendicular to the grain

Yielding of steel bracket

(d) CT3-1

Deformation of glulam column perpendicular to the grain

Yielding of steel bracket

(e) CT3-2

Fig. 8. Failure modes of the specimens under reversed cycle loading

Hysteresis curves

The moment (M)–rotation (θ) hysteresis curves for all specimens are illustrated in Fig. 9. In the initial stage of the test, all specimens showed linear-elastic behaviour. As the

applied load increased, the stiffness degraded gradually and the specimen behaviour turned into the plastic stage. As shown in Fig. 9, the shape of the hysteresis curves of group CT1 specimens exhibited reversed 'S' curves with obvious pinching effect, and there were no evident descending portions in the curves. As to groups CT2 and CT3 specimens with steel brackets, they showed less pinching effect and better rotation capacity, resulting in a better energy dissipation performance. However, the introduction of the steel brackets decreased both the load-carrying capacity and the initial rotation stiffness. These properties can be designed and optimized by the adjustment of the size and type of the steel brackets.
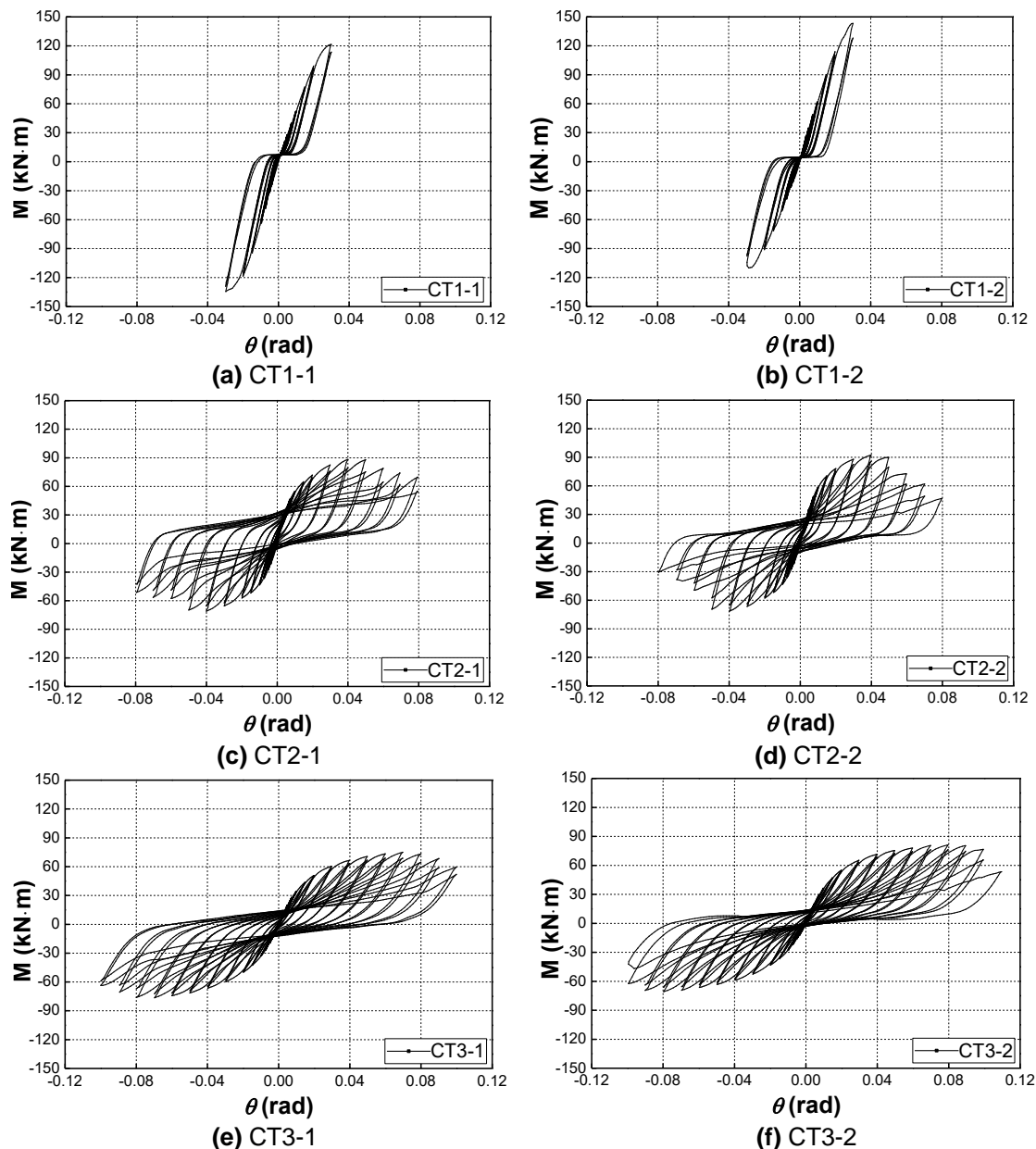
Fig. 9. Moment (M)–rotation (θ) hysteresis curves

Envelope curves

The envelope curves were obtained by enveloping the M-θ curves of the first loading cycle at each rotation level, as shown in Fig. 10. The main test results of all specimens are shown in Table 4, where the positive direction and the negative direction represent push and pull, respectively. The definition of typical parameters of the envelope curves also refer to Fig. 7 (EN 12512 2001). As compared the test results in Table 4 to Table 3, the following observations can be drawn:

- There was no obvious difference for the yielding rotation under both static loads and reversed cycle loads. However, the maximum rotation under reversed cycle loads was much smaller than that under static loads. For example, the maximum rotation of CT2 groups was only 37% that of MT2 group.
- For the specimens with steel brackets, the ultimate moment showed little differences. Consequently, the application of steel bracket can obviously decline the discreteness of the connection.
- When compared with the specimens under static loads, the initial rotation stiffness decreased by 10% to 30% for the specimens under reversed cycle loads.
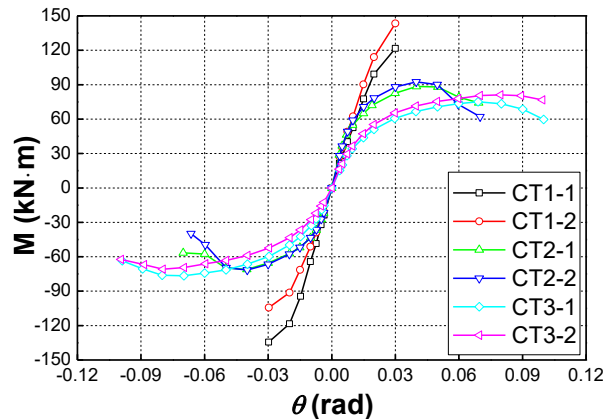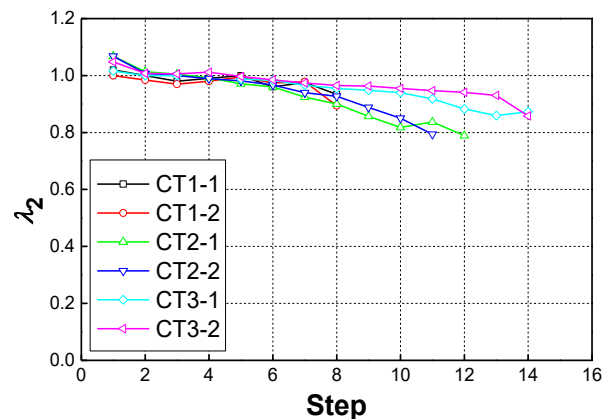

Fig. 10. The envelope curves

Fig. 11. Degradation of strength

Table 4. The Main Results of the Reversed Cycle Loading Test

Test specimen		CT1-1	CT1-2	CT2-1	CT2-2	CT3-1	CT3-2
θ_y (rad)	Positive	0.019	0.018	0.010	0.011	0.014	0.009
	Negative	-0.012	-0.012	-0.010	-0.010	-0.015	-0.014
M_y (kN·m)	Positive	98.0	112.1	63.1	69.4	52.7	42.8
	Negative	-104.0	-79.7	-49.9	-50.5	-50.2	-43.2
θ_{max} (rad)	Positive	0.030	0.030	0.040	0.040	0.070	0.080
	Negative	-0.030	-0.030	-0.040	-0.040	-0.070	-0.080
M_{max} (kN·m)	Positive	121.6	143.4	88.4	92.5	75.1	81.2
	Negative	-134.4	-104.3	-71.0	-71.5	-75.5	-70.8
k_s (kN·m /rad)	Positive	4919	5495	5977	6843	3227	3268
	Negative	6688	5176	4917	4836	2922	2502
μ	Positive	1.61	1.65	7.58	5.55	6.92	11.9
	Negative	2.49	2.53	7.12	5.68	6.98	7.76

Degradation of strength

The strength degradation of the test specimens was evaluated by the strength degradation coefficient λ_i at same loading according to Chinese standard (JGJ/T101 2015). The strength degradation coefficient λ_i is defined by Eq. 2,

$$\lambda_i = \frac{F_j^i}{F_j^{i-1}} \tag{2}$$

where F_j^{i-1} and F_j^i is the maximum load of the i-1th (ith) loading cycle at the jth loading step.

The strength degradation curves in the second loading cycle are shown in Fig. 11. The strength degradation coefficient λ_2 remained stable and ranged mostly from 0.9 to 1.1. This reveals that it achieved a good compatibility among the joint components such as the threaded rods, the steel brackets, and even the beam elements, *etc*.

Degradation of stiffness

To reflect the stiffness of the structure under reversed cycle loading, the secant stiffness referring to Chinese standard (JGJ/T 101 2015) was used to calculate the rotational stiffness of connection, as shown in Eq. 3,

$$K_i = \frac{\left|+M_i\right| + \left|-M_i\right|}{\left|+\theta_i\right| + \left|-\theta_i\right|} \tag{3}$$

where K_i is the secant stiffness of the ith primary cycle (kN·m/rad), M_i is the maximum moment of the ith primary cycle (kN·m), and θ_i is the rotation corresponding to the maximum moment of the ith primary cycle (rad).
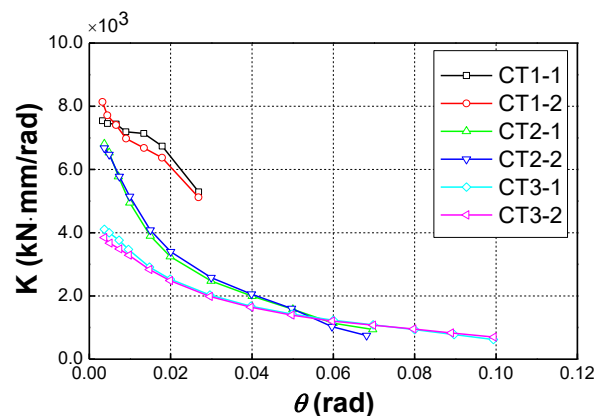

Fig. 12. Degradation of stiffness

The stiffness degradation curves of the specimens under reversed cycle loading are illustrated in Fig. 12. The stiffness degradation of the specimens results from yielding of the threaded rods, yielding of the steel brackets, and deformation of glulam column perpendicular to the grain.

Ductility

Ductility is an important factor in structure under seismic action. Herein, ductility factor, which is calculated by Eq. (1), was used to evaluate the ductility of structure. Test results of the ductility factor are listed in Tables 3 and 4.

Tables 3 and 4 show that the ductility factor of connection is significantly increased by introducing the steel brackets. The average ductility factor of group CT2 specimens, which reached to 6.5, was 3.13 times that of group CT1. For group CT3 specimens, the average ductility factor was even higher and reached to 8.4. It was considered as a result of the contribution of the deformation of glulam column perpendicular to the grain.

Energy dissipation

According to the JGJ/T101 (2015) standard, the idealized load versus deflection relationship may be illustrated as shown in Fig. 13. The equivalent viscous damping coefficient ξ_{eq} may be estimated by Eq. 4. Herein, S_{ABC} and S_{CDA} refer to the upper half area and lower half area of the hysteresis curve, respectively. $S_{\Delta OBE}$ and $S_{\Delta ODF}$ refer to the corresponding triangular areas.

$$\xi_{eq} = \frac{1}{2\pi} \cdot \frac{(S_{ABC} + S_{CDA})}{(S_{\Delta OBE} + S_{\Delta ODF})} \tag{4}$$

The curve of equivalent viscous damping coefficient in reversed cycle loading test is presented in Fig. 14. Thus, the steel brackets were able to greatly improve the energy dissipating capability of the connection. Moreover, in most cases, the equivalent viscous damping coefficient of Group CT2 specimens were much higher than that of Group CT3 specimens. This is mainly because that the steel column had quite smaller deformation than the glulam column.
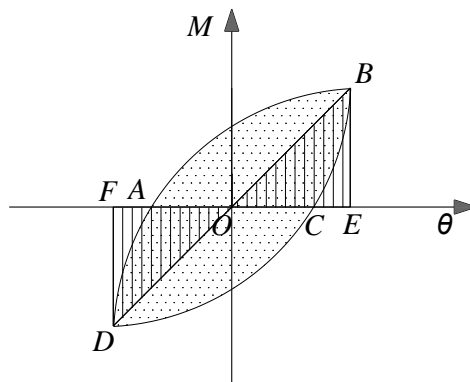

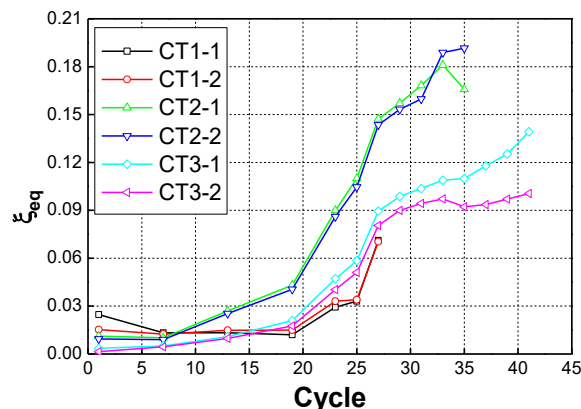**Fig. 13.** Energy dissipation determination

Fig. 14. Coefficient of equivalent viscous damping

CONCLUSIONS

1. Screwed-in threaded rod joints showed excellent structural performances when used in moment-resisting connections for timber structures. Moreover, compared with glued-in rod joints, they have better quality control performance and higher durability.

2. By combining screwed-in threaded rod and steel bracket, the resultant hybrid joints feature large stiffness, high load-carrying capacity, remarkable ductility, and good energy dissipation capacity. In addition, they allow a practical application and easy assembly.

3. The structural bearing capacity of the hybrid joints could be well designed and optimized through the design of the basic parameters of both threaded rods and steel brackets. As a result, the failure modes of the glulam beam-to-column connections are all ductile, in which the failure is mainly caused by the yielding of steel brackets, as well as the yielding or rupture of the threaded rods, which can be well designed.

4. Due to the microscopic damage caused by the cyclic loads, the load-carrying capacity, stiffness, yield rotation and maximum rotation of the connections under the reversed cycle loading are smaller than those under the static loading.

5. The mechanical properties of column have great influence on the rotation stiffness of the beam-to-column connection. As compared with specimens MT2 (using H-section steel column), the specimens MT3 (using glulam column) showed the 42.6% decline in initial rotation stiffness, due to the relatively weak compressive resistance of glulam perpendicular to the grain.

ACKNOWLEDGMENTS

REFERENCES CITED

Araki, Y., Endo, T., and Iwata, M. (2011). "Feasibility of improved slotted bolted connection for timber moment frames," *Journal of Wood Science* 57(3), 247-253. DOI: 10.1007/s10086-010-1165-7

Buchanan, A. H., and Fairweather, R. H. (1993). "Seismic design of glulam structures," *Bulletin of the New Zealand Society for Earthquake Engineering* 26(4), 415-436.

Clark, P., Frank, K., Krawinkler, H., and Shaw, R. (1997). *Protocol for Fabrication, Inspection, Testing and Documentation of Beam-column Connection Tests and Other Experimental Specimens*, SAC Joint Venture.

EN 12512 (2001). "Timber structures – Test methods – Cyclic testing of joints made with mechanical fasteners," European Committee for Standardization, Brussels, Belgium.

Fragiacomo, M., and Batchelar, M. (2012a). "Timber frame moment joints with glued-in steel rods. II: Experimental investigation of long-term performance," *Journal of Structural Engineering* 138(6), 802-811. DOI: 10.1061/(ASCE)ST.1943-541X.0000517

Fragiacomo, M., and Batchelar, M. (2012b). "Timber frame moment joints with glued-in steel rods. I: Design," *Journal of Structural Engineering* 138(6), 789-801. DOI: 10.1061/(ASCE)ST.1943-541X.0000419

GB/T 50017 (2017). "Standard for design of steel structures," Standardization Administration of China, Beijing, China.

Jensen, J. L., Nakatani, M., Quenneville, P., and Walford, B. (2012). "A simplified model for withdrawal of screws from end-grain of timber," *Construction and Building Materials* 29, 557-563. DOI: 10.1016/j.conbuildmat.2011. 10.066

JGJ/T 101 (2015). "Specification for seismic test of buildings," Architecture and Building Press, Beijing, China.

Komatsu, K., Morimoto, T., Kurumada, S., Tanaka, H., Shimizu, T., Kawahara, S., Akiyama, N., and Nakatani, M. (2018). "Development of glulam moment-resisting joint having high initial stiffness, clear yielding moment and rich ductility," in: *Proceedings of the 15th World Conference on Timber Engineering*, Seoul, Republic of Korea.

Lam, F., Closen, M., and Gehloff, M. (2010). "Moment-resisting bolted timber connections," *Structures* and *Buildings* 163(4), 267-274. DOI: 10.1680/stbu.2010.163.4.267

Leijten, A. J. M. (2011). "Requirements for moment connections in statically indeterminate timber structures," *Engineering Structures* 33(11), 3027-3032. DOI: 10.1016/j.engstruct.2011.03.014

Li, Z., Luo, J., He, M. J., Yu, X. S., Liang, F., Shu, Z., and Sun, Y. L. (2021). "Analytical investigation into the rotational behavior of glulam bolted connections with slotted-in steel plates under coupled bending moment and shear force," *China Civil Engineering Journal* 33(11), 1-12.

Liu, W. Q., and Yang, H. F. (2019). "Research progress on modern timber structures," *Journal of Building Structures* 40 (2), 16-43. DOI: 10.14006/j.jzjgxb.2019.02.002

Mori, T., Nakatani, M., and Tesfamariam, S. (2015). "Performance of semirigid timber frame with Lagscrewbolt connections: Experimental, analytical, and numerical model results," *International Journal of Advanced Structural Engineering* 7(4), 387-403. DOI: 10.1007/s40091-015-0107-4

Nakatani, M., Mori, T., and Komatsu, K. (2006). "Development of moment-resisting joint systems using lagscrewbolts," in: *Proceedings of the 9th World Conference on Timber Engineering*, Portland, USA.

Stamatopoulos, H., and Malo, K. A. (2015). "Withdrawal capacity of threaded rods embedded in timber elements," *Construction and Building Materials* 94, 387-397. DOI: 10.1016/j.conbuildmat.2015.07.067

Stamatopoulos, H., and Malo, K. A. (2016). "Withdrawal stiffness of threaded rods embedded in timber elements," *Construction and Building Materials* 94, 263-272. DOI: 10.1016/j.conbuildmat.2016.04.144

Stamatopoulos, H., and Malo, K. A. (2018). "Withdrawal of pairs of threaded rods with small edge distances and spacings," *European Journal of Wood and Wood Products* 76 (1), 31-42. DOI: 10.1007/s00107-016-1146-7

Stamatopoulos, H., and Malo, K. A. (2020). "On strength and stiffness of screwed-in threaded rods embedded in softwood," *Construction and Building Materials* 261, 119999. DOI: 10.1016/j.conbuildmat.2020.119999

Vašek, M., and Vyhnálek, R. (2006). "Timber semi rigid frame with glued-in-rods joints," in: *Proceedings of the 9ᵗʰ World Conference on Timber Engineering*, Portland, USA.

Wang, M. Q., Song, X. B., Gu, X. L., Zhang, Y. F., and Luo, L. (2015). "Rotational behavior of bolted beam-to-column connections with locally cross-laminated glulam," *Journal of Structural Engineering* 141(4). Article ID 04014121. DOI: 10.1061/(ASCE)ST.1943-541X.0001035

Xu, B. H., Bouchaïr A., Taazount M., and Vega, E. J. (2009). "Numerical and experimental analyses of multiple-dowel steel-to-timber joints in tension perpendicular to grain," *Engineering Structures* 31(10), 2357-2367. DOI: 10.1016/j.engstruct.2009.05.013

Yang, H. F., Liu, W. Q., and Ren, X. (2016). "A component method for moment-resistant glulam beam-column connections with glued-in steel rods," *Engineering Structures* 115, 42-54. DOI: 10.1016/j.engstruct.2016.02.024

Yang, H. F., Ji, J. F., Tao, H. T., Shi, B. K., Hu, J. B., and Wen, B. (2021). "Pull-out behaviour of axially loaded screwed-in threaded rods embedded in CLT elements: Experimental study," *Journal of Renewable Materials*. DOI: 10.32604/jrm.2021.016118